ChemComm

Significantly Enhanced CO Oxidation Activity Induced by CO Adsorption Site Change on Pd Nanoparticles Covered with Metal−Organic Framework

Journal:	*ChemComm*
Manuscript ID	CC-COM-01-2020-000566.R1
Article Type:	Communication

COMMUNICATION

Significantly Enhanced CO Oxidation Activity Induced by CO Adsorption Site Change on Pd Nanoparticles Covered with Metal—Organic Framework

Received 00th January 20xx,
Accepted 00th January 20xx

DOI: 10.1039/x0xx00000x

Yoshimasa Aoyama,[a] Hirokazu Kobayashi,*[a,b] Tomokazu Yamamoto,[c] Takaaki Toriyama,[d] Syo Matsumura,[c,d,e] Masaaki Haneda,[f,g] and Hiroshi Kitagawa*[a,e,h]

We report significantly enhanced CO oxidation activity of Pd nanoparticles covered with $[Zr_6O_4(OH)_4(BDC)_6]$ (UiO-66, BDC = 1,4-benzenedicarboxylate). The catalytic activity was much higher than those of Pd and Ru nanoparticles on ZrO_2. The origin of enhancement was suggested to be a change in the CO adsorption property on Pd nanoparticles.

CO oxidation on metal is very important not only in fundamental science but also in a wide range of industrial fields, including automobiles and fuel cell systems.[1] The Pt-group metals, such as Pd, Rh, Ru, and Pt, are representative CO oxidation catalysts.[2–4] In particular, Pt and Pd have been investigated extensively and the CO adsorption properties or the CO oxidation mechanism are well understood.[5] The CO adsorption properties, such as adsorption strength and site activity on a metal surface, are basically due to CO σ-donation to metal and metal π-back donation to CO.[6] As the adsorption properties strongly depend on the electronic interaction between CO and the metal surface, attempts to develop useful CO oxidation catalysts have typically involved metal alloying[7] with other elements and/or metal oxide support modification[8] for metal–support interaction.

[a] *Division of Chemistry, Graduate School of Science, Kyoto University, Kitashirakawa-Oiwakecho, Sakyo-ku, Kyoto, 606-8502, Japan. E-mail: kitagawa@kuchem.kyoto-u.ac.jp*
[b] *PRESTO, Japan Science and Technology Agency, 4-1-8 Honcho, Kawaguchi, Saitama 332-0012, Japan*
[c] *Department of Applied Quantum Physics and Nuclear Engineering, Kyushu University, 744 Motooka, Nishi-ku, Fukuoka 819-0395, Japan*
[d] *The Ultramicroscopy Research Center, Kyushu University, 744 Motooka, Nishi-ku, Fukuoka 819-0395, Japan*
[e] *INAMORI Frontier Research Center, Kyushu University, 744 Motooka, Nishi-ku, Fukuoka 819-0395, Japan*
[f] *Advanced Ceramics Research Center, Nagoya Institute of Technology, 10-6-29 Asahigaoka, Tajimi, Gifu 507-0071, Japan*
[g] *Frontier Research Institute for Materials Science, Nagoya Institute of Technology, Gokiso-cho, Showaku, Nagoya 465-8555, Japan*
[h] *Institute for Integrated Cell-Material Sciences (iCeMS), Kyoto University, Yoshida, Sakyo-ku, Kyoto 606-8501, Japan*
Electronic Supplementary Information (ESI) available: [details of any supplementary information available should be included here]. See DOI: 10.1039/x0xx00000x

Metal–organic frameworks (MOFs), which consist of metal ions connected by organic bridging ligands to a porous structure, have attracted much research interest due to their gas storage[9,10] and separation.[11,12] Because of their high porosity and designability, MOFs have also received increasing interest as a functional support material for metal nanocatalysts. In particular, the hybrid structure in which metal nanoparticles (NPs) are covered with MOF (NP@MOF) has an advantage in fully utilizing the properties of both components.[13–16] For example, Arshad Aijaz *et al.* immobilized Pd and Pt NPs into MIL-101 for CO oxidation catalysis.[17] Gui-lin Zhuang *et al.* synthesized Pt NPs loaded in UiO-67 for CO oxidation reaction.[18] So far, most studies on the hybrid catalysts have utilized MOFs mainly as a platform for immobilizing small metal NPs to prevent aggregation of the NPs during the CO oxidation reaction.[19–21] In addition, there have been a limited number of reports comparing the catalytic activity of NP@MOF with that of NPs on a metal oxide support such as Al_2O_3 or ZrO_2.

Herein, we report on the significantly enhanced CO oxidation activity of Pd NPs covered with MOFs. The activity was much higher than that of Pd or Ru NPs on ZrO_2, which is known as the highly active CO oxidation catalysts. In-situ Fourier transform infrared (FT-IR) spectroscopy measurements suggested that the enhancement in catalytic activity originated from a change in the CO adsorption site on the surface of Pd NPs induced by the MOF coating. These results indicated for the first time that MOF coating could control the adsorption property of reactants on metal NPs.

As the MOF coating on Pd NPs, we selected a Zr-based MOF, $[Zr_6O_4(OH)_4(BDC)_6]$ (UiO-66, BDC = 1,4-benzenedicarboxylate) because of its high porosity, large specific surface area, and high thermal stability.[22] We synthesized the hybrid Pd@UiO-66 by a two-step synthesis. At first, Pd NPs were prepared by a chemical reduction method. An amount of 80 mL of aqueous Na_2PdCl_4 (1425 mg, 4.8 mmol) solution was added to 200 mL of aqueous solution including poly(*N*-vinyl-2-pyrrolidone) (PVP)

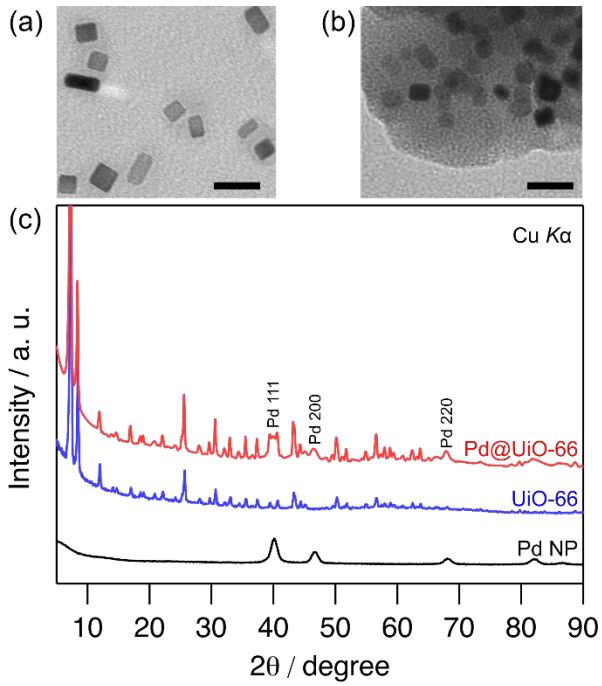

Fig. 1 TEM images of (a) Pd NPs and (b) Pd@UiO-66. Scale bar = 20 nm. (c) XRD patterns of Pd@UiO-66 (red), UiO-66 (cyan), and Pd NPs (black). The radiation wavelength was Cu-*K*α.

(1050 mg,9.5 mmol), L-ascorbic acid (1500 mg, 9.7 mmol), KBr (125 mg, 1.1 mmol), and KCl (4625 mg, 62.0 mmol). The mixture was heated at 80 °C under magnetic stirring for 3 h. After cooling to room temperature, the product was collected by centrifugation and washed twice with the mixture solution of water, acetone, and diethyl ether. For the preparation of Pd@UiO-66, we used zirconium propoxide as a precursor of UiO-66.[23,24] In typical synthesis of Pd@UiO-66, the obtained Pd NPs (30 mg) were mixed with zirconium propoxide (128.4 μL, 0.29 mmol), 1,4-benzenedicarboxylic acid (50 mg, 0.30 mmol) and acetic acid (6.5 mL) in dimethylformamide (DMF) (41 mL). The mixture was placed in an oven and heated at 65 °C for 15 h. The product was collected by centrifugation and washed with DMF twice, followed by soaking in methanol for 1 day three times. For reference, ZrO_2 supported Pd NPs (Pd/ZrO_2) were also prepared (see experimental procedures in ESI). From inductively coupled plasma atomic emission spectroscopy, the ratios of Pd included in the Pd@UiO-66 was estimated to be 1.0 wt%. By contrast, the ratio of Pd in the Pd/ZrO_2 was estimated to be 1.3 wt% by X-ray fluorescence measurements.

Transmission electron microscope (TEM) images showed that the mean diameter of the Pd NPs before and after UiO-66 coating was 7.7 ± 1.0 and 8.0 ± 1.0 nm, respectively, and the size of Pd NPs remained unchanged (Fig. 1a, b, Fig. S1). The mean diameter of Pd NPs in Pd/ZrO_2 was 7.8 ± 0.9 nm (Fig. S2). The powder X-ray diffraction (XRD) pattern of the composite consisted of diffractions from both the Pd NPs and UiO-66 lattice (Fig. 1c). From the Le Bail fitting of the XRD pattern for the composite, the crystal size of Pd NPs in the composite was determined to be 7.6 nm, which is similar value with the mean diameter estimated from the TEM image. The lattice constants of Pd and UiO-66 components in the composite were

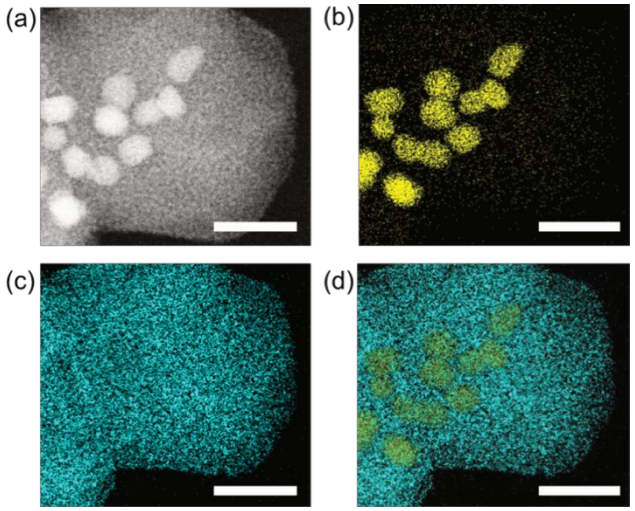

Fig. 2 (a) HAADF-STEM image and EDX maps of (b) Pd-L and (c) Zr-L obtained from Pd@UiO-66. (d) Reconstructed overlay image of the maps shown in panels (b) and (c) (cyan, Zr; yellow, Pd). Scale bar = 20 nm.

3.903(1) Å and 20.8077(8) Å, respectively (Fig. S3). These values were consistent with those of pristine Pd NPs and UiO-66 (3.8898(5) and 20.8238(5) Å, respectively), which is good agreement with previously reported values.[22,25] IR spectra (Fig. S4) and thermogravimetric measurements (Fig. S5) also confirmed the existence of UiO-66 in the composite. The N_2 sorption isotherm at 77 K for the composite showed a typical type-I sorption behavior derived from the microporosity of UiO-66 (Fig. S6).

To determine the composite states of Pd@UiO-66, we performed high-angle annular dark-field scanning TEM (HAADF-STEM) observations (Fig. 2a) and elemental mapping with energy-dispersive X-ray (EDX) spectroscopy. Fig. 2b and 2c show the EDX maps of Pd–L and Zr-L corresponding to the constituent elements of Pd NPs and UiO-66, respectively. An overlay map of the Pd–L and Zr-L is presented in Fig. 2d. These mapping revealed that the Zr elements of UiO-66 are distributed around the surface of the Pd NPs. These results indicate that Pd NPs were successfully covered with UiO-66.

To investigate the catalytic activity in CO oxidation, the catalyst that included 1.0 mg of Pd was loaded into a fix-bed flow reactor with quartz wool. A gas mixture of $CO/O_2/He$ ($CO/O_2/He$: 0.5/0.5/49 cm^3 min^{-1}) was passed over the catalysts at 35 °C, and the catalysts were then heated to 300 °C at a rate of 5 °C/min. The products were analyzed by a quadrupole mass spectrometer. The catalytic activity test was repeated five times. The temperature dependence of the CO conversion rate for Pd@UiO-66 is shown in Fig. 3a. In the first run, the temperature corresponding to 50% conversion (T_{50}) of CO to carbon dioxide (CO_2) was 225 °C, which is higher than that of Pd/ZrO_2 (200 °C) (Fig. S7a). With the repetition of the measurement, the T_{50} of Pd@UiO-66 significantly decreased, whereas that of Pd/ZrO_2 remained unchanged. The plot of T_{50} vs. the measurement cycle for Pd@UiO-66 and Pd/ZrO_2 is shown in Fig. 3b. The result for Ru NPs supported on ZrO_2 (Ru/ZrO_2) was also plotted (Fig. S7b).

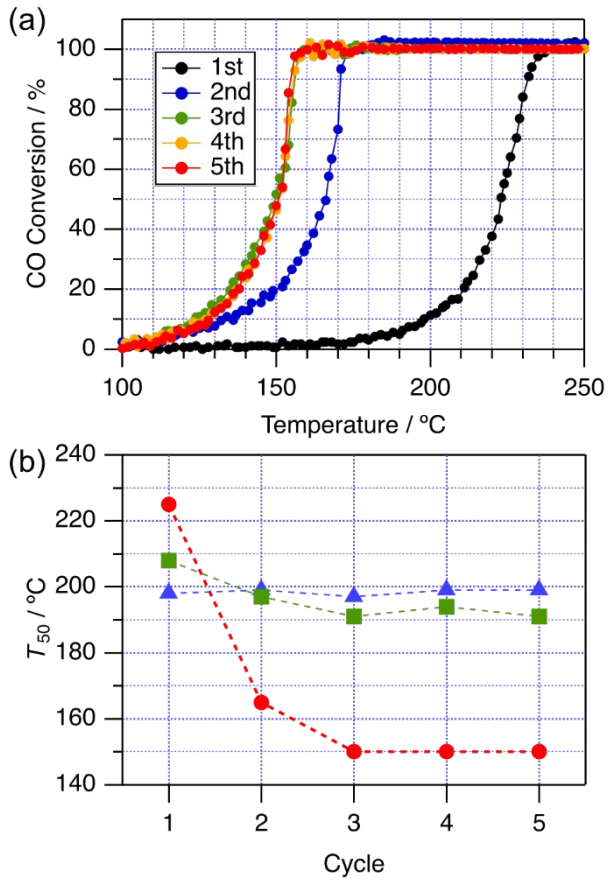

Fig. 3. (a) CO conversion rate of Pd@UiO-66. The reactions were carried out under at a flow of 1% CO/1% O_2/He with a total flow rate of 50 cm^3/min STP. (b) The T_{50} vs. measurement cycle for Pd@UiO-66 (red), Pd/ZrO_2 (blue) and Ru/ZrO_2 (green).

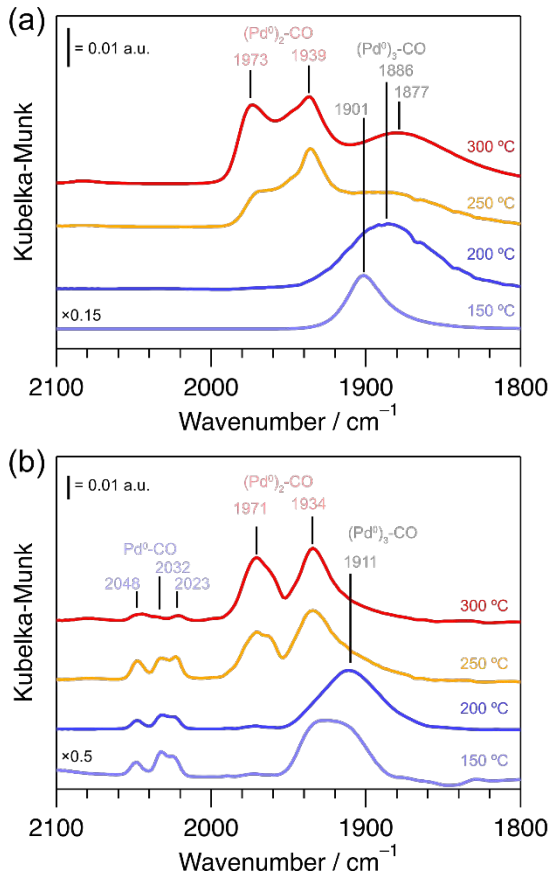

Fig. 4. In-situ IR spectra for (a) Pd/ZrO_2 and (b) Pd@UiO-66 under 0.3% CO/He flow. The four spectra were obtained at 50 °C after pretreatment at 150 °C (cyan), 200 °C (blue), 250 °C (orange) and 300 °C (red).

In the first cycle, the CO oxidation activity of Pd@UiO-66 (T_{50} = 225 °C) was lower than that of either Pd/ZrO_2 (T_{50} = 200 °C) or Ru/ZrO_2 (T_{50} = 208 °C). Surprisingly, the second cycle measurement showed a drastic enhancement of CO oxidation activity for Pd@UiO-66. Finally, the T_{50} of Pd@UiO-66 was 150 °C in the fifth cycle, whereas the results for Pd/ZrO_2 and Ru/ZrO_2 were 200 and 190 °C, respectively. These results indicated that Pd@UiO-66 exhibited excellent catalytic activity with T_{50} lower by 40 K than that of Ru NPs. The enhanced CO oxidation activity of Pd@UiO-66 is slightly higher than that of the best monometallic catalyst of face-centered cubic (fcc) Ru NPs.[26] The drastic enhancement in CO oxidation activity for Pd@UiO-66 was reproduced with another sample (Fig. S8). The pristine structure of the composite, including the mean diameter of Pd NPs, and the crystallinity and porosity of UiO-66 were maintained after the CO oxidation measurements (Fig. S6 and S9). Considering that the enhancement of CO oxidation activity was not observed by pretreatment at 300 °C under He flow (Fig.S10), both high temperature and reaction gas are important to enhance the catalytic activity. It should be also noted that Pd NPs supported on UiO-66 and Pd NPs coated with 1,4-benzenedicarboxylic acid exhibited much lower CO oxidation activity than Pd@UiO-66 (Fig. S11 and 12). Therefore, UiO-66 coating on Pd NPs contribute to the improvement of catalytic activity of Pd NPs.

To discuss the origin of the significant enhancement in CO oxidation activity of Pd@UiO-66 shown in Fig. 3, we measured the FT-IR spectra of CO adsorbed on Pd/ZrO_2 and Pd@UiO-66. The samples were pretreated under the reaction gas at 150, 200, 250, and 300 °C. After the pretreatment, the samples were cooled to 50 °C and FT-IR measurements were carried out under CO gas flow. For Pd/ZrO_2 pretreated at 150 and 200 °C, absorption bands assignable to hollow-bonded CO on Pd atoms were observed at 1901 cm^{-1} for 150 °C and 1886 cm^{-1} for 200 °C (Fig. 4a).[27] With higher temperature pretreatments, at 250 and 300 °C, new IR bands appeared, which were assignable to bridge-bonded CO (1970 to 1930 cm^{-1}) on the Pd surface.[27] However, the hollow-bonded CO bands still remained. For Pd@UiO-66, linear-bonded CO bands (2050 to 2020 cm^{-1})[27] were observed at 150 and 200 °C, in addition to hollow-bonded CO bands, as with Pd/ZrO_2 (Fig. 4b). Interestingly, at 250 and 300 °C, hollow-bonded CO bands disappeared, and linear and bridge-bonded CO bands became major. These pretreatment temperatures correspond to the temperature where the conversion of CO to CO_2 reaches 100%. Therefore, the activity enhancement of Pd@UiO-66 observed from the second cycle (Fig. 3a) was considered to have originated from the CO

adsorption site change on Pd NPs, caused by the high temperature treatment. In fact, we confirmed that the linear and bridge-bonded CO on Pd NPs are reactive for the oxidation reaction by time-dependent in-situ FT-IR measurements of Pd@UiO-66 (Fig. S13).

The in-situ FT-IR spectra in Fig. 4 suggested that the enhancement of oxidation activity for Pd@UiO-66 correlated to the change of the CO adsorption site on Pd NPs caused by MOF coating with high temperature treatments. It is considered that the CO oxidation over a Pd surface follows the Langmuir−Hinshelwood mechanism: a coadsorbed O atom and a CO molecule react on the metal surface.[5] The CO molecules at hollow sites are strongly stabilized due to the π-back donation from the metal to the CO molecule, and the reactivity of the adsorbed CO is expected to be much lower than that of CO adsorbed at top and bridge sites.[28,29] Therefore, for Pd@UiO-66, the CO adsorption site changed from a hollow to a bridge or top site on Pd NPs potentially contributed to the enhanced CO oxidation activity, while the catalytic activity of Pd/ZrO_2 remained unchanged due to the existence of hollow-bonded CO molecules. In addition, an electronic interaction between Pd NPs and UiO-66 was not observed from X-ray photoelectron spectroscopy before and after the CO oxidation reaction (Fig. S14). Hence, the enhancement of CO oxidation activity should be attributed to a reconstruction at the interface between Pd NPs and UiO-66, i.e. the Zr_6 cluster or BDC ligand of UiO-66 may block hollow sites for CO adsorption on Pd NPs. The detail mechanism on the CO adsorption change via 1st cycle of CO oxidation is under investigation, including theoretical calculation.

In summary, we obtained a significantly enhanced CO oxidation activity of Pd NPs covered with UiO-66. The activity of Pd@UiO-66 was much higher than those of Pd/ZrO_2 or Ru/ZrO_2. In addition, the activity was also superior to the fcc Ru NPs reported as the best monometallic CO oxidation catalyst. The origin of the enhancement of CO oxidation activity was suggested to be a CO adsorption site change from a hollow to a bridge or top site on Pd NPs. These results give the first example of control of the adsorption property of reactants on metal NPs by an MOF coating. We hope that these new findings will contribute to further development of useful MOF-based metal catalysts for reactions related to the CO molecule.

This work was supported by the Japan Science and Technology Agency (JST) PRESTO (No. JPMJPR1514), the Japan Society for the Promotion of Science (JSPS) Grants-in-Aid for Scientific Research (B) (No. 17750056), Core Research for Evolutional Science and Technology (CREST) and ACCEL from JST, and Grants-in-Aid for JSPS Fellows (JP 17J10102) from JSPS. STEM observations were performed as part of a program conducted by the Advanced Characterization Nanotechnology Platform sponsored by MEXT, Japan.

Conflicts of interest

There are no conflicts to declare.

Notes and references

1 G. Ertl, *Angew. Chem. Int. Ed.*, 2008, **47**, 3524–3535.
2 H. S. Gandhi, G. W. Graham and R. W. McCabe, *J. Catal.*, 2003, **216**, 433–442.
3 A. Russell and W. S. Epling, *Catal. Rev.*, 2011, **53**, 337–423.
4 F. Haaß and H. Fuess, *Adv. Eng. Mater.*, 2005, **7**, 899–913.
5 K. Liu, A. Wang and T. Zhang, *ACS Catal.*, 2012, **2**, 1165–1178.
6 G. Doyen and G. Ertl, *Surf. Sci.*, 1974, **43**, 197–229.
7 K. Kusada, H. Kobayashi, R. Ikeda, Y. Kubota, M. Takata, S. Toh, T. Yamamoto, S. Matsumura, N. Sumi, K. Sato, K. Nagaoka and H. Kitagawa, *J. Am. Chem. Soc.*, 2014, **136**, 1864–1871.
8 J. R. Gaudet, A. de la Riva, E. J. Peterson, T. Bolin and A. K. Datye, *ACS Catal.*, 2013, **3**, 846–855.
9 M. Eddaoudi, J. Kim, N. Rosi, D. Vodak, J. Wachter, M. O'Keeffe and O. M. Yaghi, *Science*, 2002, **295**, 469–472.
10 N. L. Rosi, J. Eckert, M. Eddaoudi, D. T. Vodak, J. Kim, M. O'Keeffe and O. M. Yaghi, *Science*, 2003, **300**, 1127–1129.
11 O. M. Yaghi, G. Li and H. Li, *Nature*, 1995, **378**, 703–706.
12 J.-R. Li, R. J. Kuppler and H.-C. Zhou, *Chem. Soc. Rev.*, 2009, **38**, 1477–1504.
13 G. Li, H. Kobayashi, J. M. Taylor, R. Ikeda, Y. Kubota, K. Kato, M. Takata, T. Yamamoto, S. Toh, S. Matsumura and H. Kitagawa, *Nat. Mater.*, 2014, **13**, 802–806.
14 Y. Zhao, N. Kornienko, Z. Liu, C. Zhu, S. Asahina, T.-R. Kuo, W. Bao, C. Xie, A. Hexemer, O. Terasaki, P. Yang and O. M. Yaghi, *J. Am. Chem. Soc.*, 2015, **137**, 2199–2202.
15 K. Na, K. M. Choi, O. M. Yaghi and G. A. Somorjai, *Nano Lett.*, 2014, **14**, 5979–5983.
16 G. Li, S. Zhao, Y. Zhang and Z. Tang, *Adv. Mater.*, 2018, **30**, 1800702.
17 A. Aijaz, T. Akita, N. Tsumori and Q. Xu, *J. Am. Chem. Soc.*, 2013, **135**, 16356–16359.
18 G. Zhuang, J. Bai, X. Zhou, Y. Gao, H. Huang, H. Cui, X. Zhong, C.-L. Zhong and J. Wang, *Eur. J. Inorg. Chem.*, 2017, **2017**, 172–178.
19 M. S. El-Shall, V. Abdelsayed, A. E. R. S. Khder, H. M. A. Hassan, H. M. El-Kaderi and T. E. Reich, *J. Mater. Chem.*, 2009, **19**, 7625–7631.
20 H.-L. Jiang, B. Liu, T. Akita, M. Haruta, H. Sakurai and Q. Xu, *J. Am. Chem. Soc.*, 2009, **131**, 11302–11303.
21 J. M. Zamaro, N. C. Pérez, E. E. Miró, C. Casado, B. Seoane, C. Téllez and J. Coronas, *Chem. Eng. J.*, 2012, **195–196**, 180–187.
22 J. H. Cavka, S. Jakobsen, U. Olsbye, N. Guillou, C. Lamberti, S. Bordiga and K. P. Lillerud, *J. Am. Chem. Soc.*, 2008, **130**, 13850–13851.
23 K. Tulig and K. S. Walton, *RSC Adv.*, 2014, **4**, 51080–51083.
24 M. R. DeStefano, T. Islamoglu, S. J. Garibay, J. T. Hupp and O. K. Farha, *Chem. Mater.*, 2017, **29**, 1357–1361.
25 O. Seo, J. Kim, A. Tayal, C. Song, L. S. R. Kumara, S. Dekura, H. Kobayashi, H. Kitagawa and O. Sakata, *RSC Adv.*, 2019, **9**, 21311–21317.
26 K. Kusada, H. Kobayashi, T. Yamamoto, S. Matsumura, N. Sumi, K. Sato, K. Nagaoka, Y. Kubota and H. Kitagawa, *J. Am. Chem. Soc.*, 2013, **135**, 5493–5496.
27 D. Tessier, A. Rakai and F. Bozon-Verduraz, *J. Chem. Soc. Faraday Trans.*, 1992, **88**, 741–749.
28 K. Murata, E. Eleeda, J. Ohyama, Y. Yamamoto, S. Arai and A. Satsuma, *Phys. Chem. Chem. Phys.*, 2019, **21**, 18128–18137.
29 S. N. Pavlova, V. A. Sadykov, V. A. Razdobarov and E. A. Paukshtis, *J. Catal.*, 1996, **161**, 507–516.

